2021 IEEE 18th International Symposium on Biomedical Imaging (ISBI)
April 13-16, 2021, Nice, France

VALIDATION OF A BI-ENERGETIC SPECTRUM APPROXIMATION IN BONE MINERAL DENSITY MEASUREMENT WITH A DXA DIGITAL TWIN

Karine Haddadi[⋆†], *Serge Muller*[⋆], *Isabelle Bloch*[†‡]
[⋆] GE Healthcare, Buc, France
[†] LTCI, Télécom Paris, Institut Polytechnique de Paris, France
[‡] Sorbonne Université, CNRS, LIP6, Paris, France

2021 IEEE 18th International Symposium on Biomedical Imaging (ISBI) | 978-1-6654-1246-9/20/$31.00 ©2021 IEEE | DOI: 10.1109/ISBI48211.2021.9433940

ABSTRACT

Modern DXA (Dual Energy X-ray Absorptiometry) equipments allow both quantifying compositional and geometrical features on images with high accuracy, such as bone mineral density (BMD), and measuring beaking associated with atypical femur fractures (AFF). There is a need for developing DXA digital twins to optimize the design of clinical applications quantifying features from images. This paper presents our advances in developing a digital twin of a DXA system. This digital twin leverages the CatSim simulation platform initially developed by General Electric Global Research Center for CT imaging, and allowing for realistic image simulations. Using an analytical model, we simulate the physics of the DXA X-ray acquisition chain, including X-ray source, detector, scanning geometry and image generation. Our main contribution addresses the compromise between accuracy and computation burden. Indeed, simulations can be computationally intensive when considering poly-chromatic spectra. We demonstrate in this paper that the BMD accuracy is not significantly impacted when simulating a bi-chromatic X-ray source instead of a full polychromatic source, while the computation is faster. Our results indicate a similar BMD accuracy ($error < 0.1\%$) and a reduced computation time (-44%) when using a bi-chr omatic X-ray spectrum.

***Index Terms*—** Dual Energy X-ray absorptiometry, digital twin, X-ray spectrum.

1. INTRODUCTION

Four million fragility fractures occur every year in Europe [1]. Bone fracture related to osteoporosis is an actual underestimated public health problem. The current screening strategy for osteoporosis assessment is to perform bone mineral density (BMD) measurements in selected skeleton sites. BMD is a reliable estimator for osteoporosis and fracture risk assessment [2], and is used in T-score and Z-score calculations that are determinant for osteoporosis diagnosis [3, 4]. Therefore, BMD represents a criterion of interest to assess the accuracy of simulations.

BMD measurements are commonly performed with Dual Energy X-ray Absorptiometry systems (DXA). A DXA scanner allows acquiring images at two different energies: low energy (LE) and high energy (HE). In this modality, LE and HE images are combined to calculate a bone equivalent image used for BMD measurement. In the same way, CatSim [5], our simulation platform, is able to generate LE and HE images. This simulation environment was previously used for CT [6] and mammographic imaging simulation [7, 8, 9]. CatSim provides a way to simulate each part of the acquisition chain with a given level of realism. The acquisition chain can be broken down into three main parts: the X-ray source, the simulated patient and the energy-discriminating X-ray detector. This paper presents our advances in DXA digital twins development using this simulation platform, and is specifically focusing on the validation of the simulated X-ray source. As a first step, we chose to simplify some elements of the chain, by assuming a perfect detector and using a simulated assurance quality phantom in place of a patient.

An important step in image generation with a DXA digital twin is to have an available spectrum model preserving BMD accuracy while allowing for fast simulations. Our main contribution is therefore to demonstrate the relevance of using a simple bi-energetic spectrum in our simulations instead of a full poly-energetic spectrum. In Section 2 we will validate the adequacy of our simulated poly-energetic spectrum with the real spectrum of an iDXA system (GE Healthcare, Chicago, IL, USA). Then, we will validate the adequacy of our simulated bi-energetic spectrum with the simulated poly-energetic spectrum. In Section 3, we will verify that our simulated bi-energetic spectrum enables accurate measurements of BMD on phantoms, compared to the typical expected accuracy of BMD on real DXA systems. Results will be presented in Section 4 and discussed.

2. SPECTRUM MODEL VALIDATION USING HVL CRITERION

To validate the adequacy between spectra (both real and simulated), we propose to compare their half-value layers (HVL), a commonly used criterion for spectrum model assessment [10, 11, 12, 13]. The HVL characterizes an X-ray beam in terms of its ability to penetrate a material of known composition [14]. It corresponds to the thickness of material necessary to divide by two an initial beam intensity.

2.1. Spectrum simulation

To simulate X-ray spectra used in DXA systems, we leveraged a spectrum simulation software developed at GE Healthcare (SpeXim) validated in previous works [15, 16]. This software implements a semi-empirical model based on Birch and Marshall model [17] for the Bremsstrahlung radiation and Cranley et al. [18] and Green and Cosslett [19] for the characteristic rays.

In this study, we simulated poly-energetic spectra presenting a fluence distribution typical of an X-ray tube with a Tungsten target filtered with $200\mu m$ Samarium as in iDXA scanners. The iDXA tube operates at a nominal voltage of 100 kVp. In our simulations, we varied the high voltage from 95 to 99.5 kVp and derived HVL of the generated spectra to determine which poly-energetic spectrum provides the best HVL match with the spectrum of the iDXA system. Then, we derived a bi-energetic spectrum based on the mean energies of the two iDXA spectrum modes. In order to define these two modes, a threshold was set at 52 keV. This threshold was chosen as the median energy of the poly-energetic spectrum, and the energy

peaks correspond to the mean energy on each side of the threshold (39 and 72 kVp) .

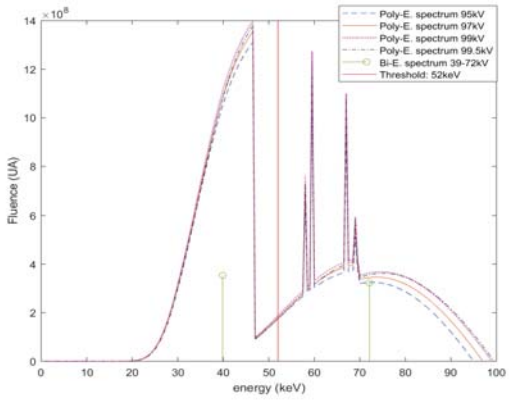

Fig. 1: Four simulated poly-energetic spectra presenting a fluence distribution typical of an X-ray tube with a Tungsten target filtered with $200\mu m$ Samarium, the energy threshold, and a bi-energetic spectrum based on mean energies of the iDXA bimodal spectum.

2.2. HVL experiment

On the physical iDXA scanner, measurements were performed with a calibrated dosimeter. Dose measurements were done according to the experimental setup illustrated in Figure 2, at a fixed distance to the source $D_{SD} = 712$ mm. The assessment of HVL [14] is based on the mean and standard deviation of five dose measurements. We also simulated the measurement of HVL on our digital twin simulating the same procedure. HVL values were derived for both the poly-energetic spectra and the bi-energetic spectrum. Results are summarized in Table 1.

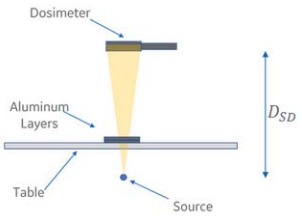

Fig. 2: Experimental set-up for HVL determination. D_{SD} is the source to dosimeter distance.

Table 1: Results of the HVL experiment.

Experimental spectrum	100kV				
HVL (mm)	5.22 [5.17-5.26]				
Simulated spectrum	95 kVp	97 kVp	99 kVp	99.5 kVp	Bi-e
HVL (mm)	5.14	5.26	5.39	5.42	5.25

Using the HVL criterion, we found that the poly-energetic spectrum at 97kV best matches the iDXA scanner spectrum. We also validated that our simulated bi-energetic spectrum provides a similar HVL (5.25mm of Al) to the HVL of both the iDXA spectrum (5.22mm of Al) and the simulated poly-energetic spectrum using a 97 kVp high voltage (5.26mm of Al). These two simulated spectra will be the ones used next, to determine the accuracy in BMD assessment using our DXA digital twin.

3. COMPARISON OF BMD DETERMINED WITH POLY- AND BI-ENERGETIC SIMULATED SPECTRA

BMD is a key measurement on a DXA system requiring a high accuracy to be clinically meaningful. In this section, we determine the BMD from simulations drawn with our iDXA digital twin. We compare the BMD values issued from simulations using the selected poly-energetic spectrum and the bi-energetic spectrum. Then, in order to validate the use of a bi-energetic spectrum in our digital twin simulations, we compare the inaccuracy introduced by using a bi-energetic spectrum instead of a poly-energetic spectrum to the expected BMD accuracy with a physical DXA scanner.

3.1. BMD calculation

From a radiology point of view, we consider that we can decompose the body into three components: bone, fat, and lean tissues. With a DXA scanner, we acquire two images: a low energy image and a high energy image. Therefore, we get two integral measures (corresponding to the log of the transmitted X-rays through the body at two different energies) to quantify the thickness of three materials in the body. To solve this undetermined problem, we consider the soft tissue as homogeneous. This means that we assume that the fat fraction (FF) in soft tissues is constant whatever the location in the body (with or without bone). Thus, the fat fraction, defined as $FF = \frac{t_{fat}}{t_{fat}+t_{lean}}$, is calculated from the whole non-bone region and the same value is used in regions containing bones. In a bi-energetic approximation, we can express the problem using the Beer-Lambert law [20], and write the LE (L) and HE (H) images as:

$$\begin{cases} L = \ln\left(\frac{I_{0L}}{I_L}\right) = \mu_{bone}(E_L)t_{bone} + \mu_{fat}(E_L)t_{fat} + \mu_{lean}(E_L)t_{lean} \\ H = \ln\left(\frac{I_{0H}}{I_H}\right) = \mu_{bone}(E_H)t_{bone} + \mu_{fat}(E_H)t_{fat} + \mu_{lean}(E_H)t_{lean} \end{cases} \quad (1)$$

where I_{0L} and I_{0H} are the incident X-ray intensities, respectively at low and high energy, I_L and I_H are the X-ray intensities after the body attenuation, μ_{bone}, μ_{fat} and μ_{lean} are the linear mass attenuations in cm^{-1} for bone, fat tissue and lean tissue, respectively, E_L and E_H are low and high energies, and t_{bone}, t_{fat} and t_{lean} are the equivalent thicknesses in cm for bone, fat and lean tissues, respectively.

In practice, to solve this system of equations, an intermediate decomposition step is necessary. From the log-corrected HE (H) and LE images (L) acquired by the DXA scanner, a pseudo bone (PBM) thickness image t_{PBM} and a pseudo soft tissue (PST) thickness image t_{PST} can be derived through a calibration process [21], leading to polynomial expressions:

$$\begin{cases} t_{PBM} = a_0 + a_1 L + a_2 H + a_3 L^2 + a_4 H^2 + a_5 LH + ... \\ t_{PST} = b_0 + b_1 L + b_2 H + b_3 L^2 + b_4 H^2 + b_5 LH + ... \end{cases} \quad (2)$$

To calculate the fat fraction, we need to know the fat and lean equivalent thickness t_{fat} and t_{lean} of each tissue. They are linearly related to t_{PBM} and t_{PST} by:

$$\begin{bmatrix} t_{fat} \\ t_{lean} \end{bmatrix} = \begin{bmatrix} A_{11} & A_{12} \\ A_{21} & A_{22} \end{bmatrix}^{-1} \begin{bmatrix} t_{PBM} \\ t_{PST} \end{bmatrix} \quad (3)$$

where A_{11} represents the fraction of fat-equivalent in pseudo-bone material, A_{12} the fraction of lean-equivalent in pseudo-bone material, A_{21} the fraction of fat-equivalent in pseudo soft tissue material, and A_{22} the fraction of lean-equivalent in pseudo soft tissue material, in a {fat, lean} basis [22].

Fat and lean equivalent thicknesses are obtained through a second calibration using materials that are surrogates of biological materials [23]. We implemented the approach proposed by Lehmann, Alvarez et al. [22] who hypothesized that mass attenuation coefficients can be expressed as a linear combination of the mass attenuation coefficients in a basis of two different materials. The two selected materials are aluminum and PMMA (poly methylmethacrylate). The X-ray mass attenuations of the materials used in our simulations were selected in the NIST database [24]. With the calculated fat fraction FF and the t_{PBM} and t_{PST} thickness values obtained through the calibration process, we can express the BMD and the soft tissue thickness t_{STD} as:

$$\begin{bmatrix} BMD \\ t_{STD} \end{bmatrix} = \begin{bmatrix} B_1 & A_{11} \times FF + A_{12} \times (1 - FF) \\ B_2 & A_{21} \times FF + A_{22} \times (1 - FF) \end{bmatrix}^{-1} \begin{bmatrix} t_{PBM} \\ t_{PST} \end{bmatrix} \quad (4)$$

where B_1 and B_2 are coefficients to express the BMD in terms of pseudo-bone and pseudo-soft materials, that are determined using a phantom with known BMD and t_{PBM} and t_{PST} thickness values. Finally we obtain:

$$BMD = \frac{D_2 \times t_{PBM} - D_1 \times t_{PST}}{B_1 \times D_2 - B_2 \times D_1} \quad (5)$$

with $D_1 = A_{11} \times FF + A_{12} \times (1 - FF)$ and $D_2 = A_{21} \times FF + A_{22} \times (1 - FF)$.

3.2. Assessment of the BMD accuracy

The simulation of the iDXA quality control phantom (QA block) provides a way to assess the BMD accuracy. The specifications of this physical phantom are known in terms of PBM and PST equivalent, fat fraction and BMD values. Our objective was to simulate the QA block, generate simulated LE and HE images and verify that the obtained PBM and PST thicknesses after simulating the calibration are in agreement with the iDXA reality. The QA block phantom (Figure 3) is composed of five chambers and four of them are used to check the BMD measurement quality (chambers 0, 2, 3 and 4). Chamber 0 is only composed with PMMA while the chambers 2, 3 and 4 are composed with a combination of PMMA and polyethersulfone. Polyethersulfone is used to simulate the bone material in this phantom and PMMA is used to simulate soft tissues.

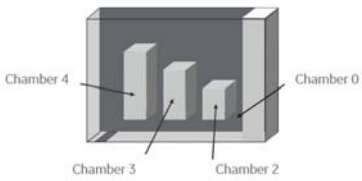

Fig. 3: A QA block schema showing the internal structures.

In the simulated PBM and PST equivalent images (Figure 4), four regions of interest were selected for each QA block chamber. Using Equations (1) and (3), ROI 0 was used to calculate the fat fraction. According to Equation (5), the BMD values of the chambers 2, 3 and 4 were calculated knowing the FF, t_{PBM} and t_{PST}

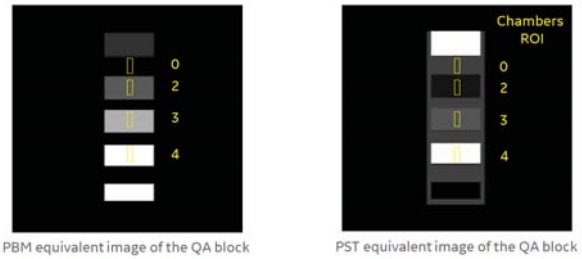

Fig. 4: Simulated PBM and PST images with ROI used to calculate BMD in each chamber.

values of each chamber. In order to compare them with the expected BMD values, we defined the relative error on BMD as:

$$R_{err(BMD)} = \frac{|\, BMDsim - BMDexp \,|}{BMDexp} \quad (6)$$

where $R_{err(BMD)}$ is the relative error on BMD (%), $BMDsim$ is a BMD value calculated with simulated images (g/cm^2) and $BMDexp$ is the specified BMD value (g/cm^2).

4. RESULTS

ROIs 2, 3, 4 were used to calculate the BMD in each chamber of the QA block. The measured BMD values on simulated images, with both poly-energetic and bi-energetic spectra, are all within the upper and acceptance values of the iDXA scanner as provided by the manufacturer (Figure 5 and Table 2). Moreover, the relative error R_{err} for BMD assessed through the simulations using a poly-energetic spectrum was 0.1% for each chamber of the QA block. We observed the same relative error for the BMD assessed through the simulations using a bi-energetic spectrum (Figure 2).

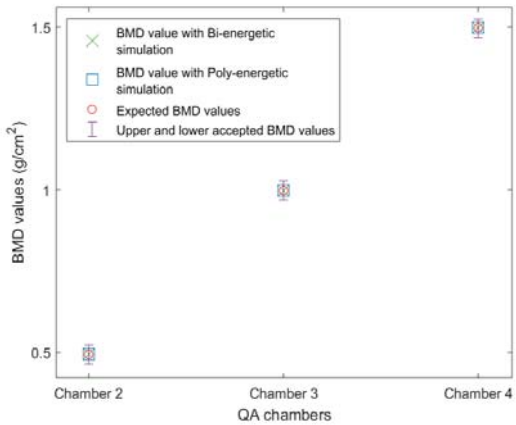

Fig. 5: BMD values for each chamber using bi-energetic and poly-energetic simulations compared to the QA block acceptance values [25].

These results show that the relative error on BMD values determined using our DXA digital twin (0.1%) is significantly lower than the required accuracy on BMD measurements required in QA acceptance tests of physical DXA systems [26]. Therefore, we validated the capability of our digital twin to derive accurate BMD values. In

Table 2: BMD values for poly and bi-energetic simulations

BMD values (g/cm^2)	Chamber 2	Chamber 3	Chamber 4
Poly-energetic simulations	0.495	0.997	1.498
Bi-energetic simulations	0.495	0.997	1.498
Expected	0.495	0.998	1.498
Acceptance	0.465-0.525	0.968-1.028	1.468-1.528

addition, the difference in BMD accuracy between poly-energetic and bi-energetic simulations is less than 0.1%. Then, using a bi-energetic spectrum in our digital twin does not degrade significantly the accuracy of the BMD, and consequently is an acceptable alternative to using a poly-energetic spectrum. Moreover, the time saving is about 44%, on the used machine (CPU: Intel(R) Xeon(R) CPU E5645 2.40GHz, 24 cores, RAM: 64GB).

5. DISCUSSION AND CONCLUSION

We demonstrated that both poly-energetic and bi-energetic spectrum models used in our DXA digital twin are leading to relative errors in BMD an order of magnitude inferior to the expected accuracy of a physical DXA scanner. In addition, we have shown that approximating the iDXA spectrum with a bi-energetic spectrum enables to assess BMD values with a very small additional error compared to simulations performed with a poly-energetic spectrum. Therefore, the use of a bi-energetic spectrum in our DXA digital twin should not degrade the densitometry in our future simulations, while allowing for a significant computation time saving compared to the poly-energetic spectrum model. The gain in computation time has been estimated so far greater than 40%. This good compromise between BMD accuracy and faster simulations is our main contribution. Nevertheless, we still observe some errors in assessing BMD values with our DXA digital twin. This may come from some assumptions made when designing our digital twin, overlooking some physical phenomena that occur in real scanners. In particular, we chose to simulate a perfect detector, leading to noiseless simulations, that could explain a part of the observed inaccuracy in BMD calculation. In future work, we will improve the realism of the simulated acquisition chain by including more realistic physical phenomena, and we will analyze the impact of noise on BMD accuracy.

6. COMPLIANCE WITH ETHICAL STANDARDS

This is a numerical simulation study for which no ethical approval was required.

7. ACKNOWLEDGEMENTS

This work was partially funded by an ANRT grant No 2019/0061. The authors would like to acknowledge Pablo Milioni de Carvalho, Rubén Sanchez de la Rosa and Ann-Katherine Carton (GE Healthcare, Buc, France) for their help in simulations and insights in X-ray physics, as well as Jim Wear and Paul Markwardt (GE Healthcare, Madison, IL, USA) for their shared expertise in DXA scanners. The authors have no relevant financial or non-financial interests to disclose.

8. REFERENCES

[1] G. Guglielmi, *Osteoporosis and bone densitometry measurements*, Springer, 2013.

[2] J.A. Kanis, "Diagnosis of osteoporosis and assessment of fracture risk," *The Lancet*, vol. 359, no. 9321, pp. 1929–1936, 2002.

[3] H.P. Dimai, "Use of dual-energy X-ray absorptiometry (DXA) for diagnosis and fracture risk assessment; WHO-criteria, T- and Z-score, and reference databases," *Bone*, vol. 104, pp. 39–43, 2017.

[4] G.M. Blake and I. Fogelman, "The role of DXA bone density scans in the diagnosis and treatment of osteoporosis," *Postgraduate Medical Journal*, vol. 83, no. 982, pp. 509–517, 2007.

[5] B. De Man, S. Basu, N. Chandra, B. Dunham, P. Edic, M. Iatrou, S. McOlash, P. Sainath, C. Shaughnessy, B. Tower, and E. Williams, "CatSim: a new computer assisted tomography simulation environment," in *SPIE Medical Imaging 2007: Physics of Medical Imaging*, 2007, vol. 6510.

[6] P. Milioni de Carvalho, A.-K. Carton, S. Saab-Puong, R. Iordache, and S. Muller, "Spectra optimization for dual-energy contrast-enhanced breast CT," in *SPIE Medical Imaging 2013: Physics of Medical Imaging*, 2013, vol. 8668.

[7] P. Milioni de Carvalho, A.-K. Carton, S. Saab-Puong, R. Iordache, and S. Muller, "Optimization of X-ray spectra for dual-energy contrast-enhanced breast imaging: Dependency on CsI detector scintillator thickness," in *International Workshop on Digital Mammography*. Springer, 2014, pp. 95–102.

[8] R. Sánchez De La Rosa, A.-K. Carton, P. Milioni de Carvalho, Z. Li, S. Muller, and I. Bloch, "Preliminary study of CEDBT and CESM performances using simulated analytical contrast uptakes," in *IEEE 15th International Symposium on Biomedical Imaging (ISBI)*, 2018, pp. 792–795.

[9] R. Sánchez De La Rosa, A.-K. Carton, P. Milioni de Carvalho, I. Bloch, and S. Muller, "Analysis of CEDBT and CESM performance using a realistic x-ray simulation platform," in *IEEE 16th International Symposium on Biomedical Imaging (ISBI)*, 2019, pp. 1070–1073.

[10] A.M. Hernandez and J.M. Boone, "Tungsten anode spectral model using interpolating cubic splines: unfiltered x-ray spectra from 20 kv to 640 kv," *Medical Physics*, vol. 41, no. 4, pp. 042101, 2014.

[11] M.R. Ay, S. Sarkar, M. Shahriari, D. Sardari, and H. Zaidi, "Assessment of different computational models for generation of X-ray spectra in diagnostic radiology and mammography," *Medical Physics*, vol. 32, no. 6, pp. 1660–1675, 2005.

[12] P. Meyer, E. Buffard, L. Mertz, A. Constantinesco, and P. Siffert, "Evaluation of the use of six diagnostic X-ray spectra computer codes," *The British Journal of Radiology*, vol. 77, no. 915, pp. 224–230, 2004.

[13] J.M. Boone and J.A. Seibert, "An accurate method for computer-generating tungsten anode X-ray spectra from 30 to 140 kV," *Medical Physics*, vol. 24, no. 11, pp. 1661–1670, 1997.

[14] J.H. Elford and C.J. Robert, *The physics of radiology*, Charles C. Thomas, Springfield, IL, 1983.

[15] S. Puong, *Imagerie du sein multispectrale avec injection de produit de contraste*, Ph.D. thesis, Université Paris Sud, Orsay, France, 2008.

[16] P. Milioni De Carvalho, *Low-dose 3D quantitative vascular X-ray imaging of the breast*, Ph.D. thesis, Université Paris Sud, Orsay, France, 2014.

[17] R. Birch and M. Marshall, "Computation of Bremsstrahlung X-ray spectra and comparison with spectra measured with a Ge (Li) detector," *Physics in Medicine & Biology*, vol. 24, no. 3, pp. 505, 1979.

[18] K. Cranley, B.J. Gilmore, G.W.A. Fogarty, and L. Desponds, "Catalogue of diagnostic X-ray spectra and other data (IPEM report 78)," *The Institute of Physics and Engineering in Medicine and Biology*, 1997.

[19] M. Green and V.E. Cosslett, "Measurements of K, L and M shell X-ray production efficiencies," *Journal of Physics D: Applied Physics*, vol. 1, no. 4, pp. 425–436, apr 1968.

[20] L. Herve, C. Robert-Coutant, J-M. Dinten, L. Verger, and V. Comparat, "Optimization of x-ray spectra for bone mineral density and body composition measurements: theoretical study and experimental validation," in *Penetrating Radiation Systems and Applications IV*. International Society for Optics and Photonics, 2002, vol. 4786, pp. 132–143.

[21] R. E. Alvarez and A. Macovski, "Energy-selective reconstructions in x-ray computerised tomography," *Physics in Medicine & Biology*, vol. 21, no. 5, pp. 733, 1976.

[22] L.A. Lehmann, R.E. Alvarez, A.M. Macovski, W.R. Brody, N.J. Pelc, A.J. Riederer, and A.L. Hall, "Generalized image combinations in dual KVP digital radiography," *Medical Physics*, vol. 8, no. 5, pp. 659–667, 1981.

[23] M.M. Goodsitt, "Evaluation of a new set of calibration standards for the measurement of fat content via DPA and DXA," *Medical Physics*, vol. 19, no. 1, pp. 35–44, 1992.

[24] H.J. Griffiths, "Tissue substitutes in radiation dosimetry and measurement. no. 4," *Radiology*, vol. 173, no. 1, pp. 202–202, 1989.

[25] "X-ray bone densitometer with encore v18 software - user manual," Tech. Rep., GE Healthcare, 2020.

[26] A. Larkin, N. Sheahan, U. O'Connor, L. Gray, A. Dowling, E. Vano, P. Torbica, D. Salat, A. Schreiner, V. Neofotistou, and J. F. Malone, "QA/acceptance testing of DEXA X-ray systems used in bone mineral densitometry," *Radiation Protection Dosimetry*, vol. 129, no. 1-3, pp. 279–283, 04 2008.